analytical chemistry

pubs.acs.org/ac Article

Gold Nanoparticles Photosensitization towards 3,4,9,10-Perylenetetracarboxylic Dianhydride Integrated with a Dual-Particle Three-Dimensional DNA Roller: A General "ON−OFF−ON" Photoelectric Plasmon-Enhanced Biosensor

Fangjing Mo, Jiang Guo, Min Chen, Hui Meng, and Yingzi Fu*

Cite This: *Anal. Chem.* 2021, 93, 10947−10954 Read Online

ACCESS | Metrics & More | Article Recommendations | Supporting Information

ABSTRACT: A high initial signal for the sensitive detection of analytes is critical in photoelectrochemical (PEC) biosensing systems. As a semiconductor, 3,4,9,10-perylenetetracarboxylic dianhydride (PTCDA) possesses an appropriate optical band gap of 2.5 eV and inherently intense and stable PEC response. When gold nanoparticles (Au NPs) are electrodeposited on the surface of PTCDA to form a Schottky junction (Au NPs/PTCDA), a surprising and satisfactory PEC performance is unfolded before our eyes. Considering the outstanding PEC behaviors of Au NPs/PTCDA and the great quenching effect of gold nanoclusters (Au NCs), the "ON−OFF−ON" PEC sensing platform has been developed for microRNA 1246 (miRNA 1246) detection combined with the cascaded quadratic amplification strategy of the polymerization/nicking reaction and dual-particle 3D DNA roller. The higher initial PEC signals of the system can be acquired by regulating the deposition time for 35 s (−0.2 V), which is derived from the synergetic effect of localized surface plasmon resonance of Au NPs and the formation of a Schottky junction. The dual-particle 3D DNA roller has been designed to guarantee wide walking space, remarkable operation performances, and inhibition of derailment. The proposed biosensor shows a dynamic range from 10 aM to 1 pM at a low detection limit of 3.1 aM and exhibits good analytical behaviors while analyzing miRNA 1246 in healthy human serum samples. This work not only expands the application of organic photoelectric materials in bioanalysis but also provides potential possibility of detecting other biomarkers by choosing appropriate target units.

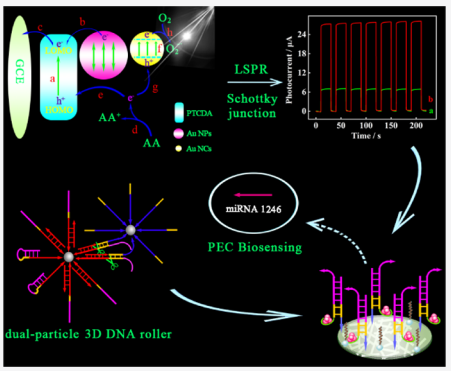

INTRODUCTION

The photoelectrochemical (PEC) method, as burgeoning analytical technology, has attracted considerable interest in the determination of biological samples. It possesses inherent merits by integrating external optical excitation and electrochemical assay systems, such as simple equipment, favorable portability, high throughput assay, and low background signals.[1,2] For "ON−OFF−ON" PEC biosensors, it is urgent to search ideal photoelectric active materials to ensure analytical sensitivity. In comparison with inorganic materials, organic materials exhibit better PEC behaviors and broader application prospects. 3,4,9,10-Perylenetetracarboxylic dianhydride (PTCDA), a large polyaromatic molecule, is one of the well-known organic semiconductors with a band gap energy of 2.5 eV, which has been used in electronic, electrochemiluminescent, and optoelectronic equipment.[3] For example, hydrazine-functionalized perylene diimide derivative supramolecular[4] and gold-doped 3,4,9,10-perylene tetracarboxylic acid (PTCA−PEI−Au)[5] have been used in PEC. Featured with recommendable membrane-forming ability, outstanding photoelectric property, and no additional synthesis process, PTCDA is gradually becoming an efficient photoelectric material.[6]

Various sensitization strategies have been developed to enhance initial PEC signals of photoactive species to ensure high analytical sensitivity. Among them, the introduction of noble metals into the semiconductor to form a Schottky junction can improve the photoreactivity and optoelectronic properties of the semiconductor.[7,8] Due to the high catalytic efficiency of gold nanoparticles (Au NPs), they can be used as an efficient photosensitizer and introduced into semiconductor substrates by electrodeposition.[9] In PEC analysis, when photons interact with Au NPs, the surface-conduction electrons collectively oscillate to generate localized surface plasmon resonance (LSPR), which can rearrange the charge

Received: April 28, 2021
Accepted: July 16, 2021
Published: July 28, 2021

https://doi.org/10.1021/acs.analchem.1c01816
Anal. Chem. 2021, 93, 10947−10954

density and establish an opposing electric field to concentrate the light energy and promote the electron movement so as to enable Au NPs own satisfactory electrochemical and electrocatalytic properties.[10,11] The Schottky junction is a notable amalgamation between semiconductors and noble-metal nanoparticles, which can promote photon-generated carrier separation via a built-in electric field. Au NPs can harvest the light of long wavelength to generate "hot electrons" and transfer to semiconductors.[12] Our group has proposed a PEC immunosensor with good analytical performances based on some Schottky junctions.[13,14] The synergetic effect of LSPR and the Schottky junction can reach a higher photoelectric conversion efficiency.[15] The properties of Au NPs including morphology, particle size, film thickness, photocatalytic efficiency, and photosensitivity efficiency are closely associated with electrodeposition conditions.[16,17] However, few literature studies involve the sensitization of Au NPs on the PEC performances of PTCDA, which has greatly aroused our interest. The superiority of quantum size makes Au NCs show larger specific surface area and molecule-like performances. Contrary to the properties of Au NPs, gold nanoclusters (Au NCs) show quenching effect toward some photoelectric materials.

MicroRNAs (miRNAs) are a category of short, noncoding, and endogenous RNAs, which serve as significant post-transcriptional regulators in gene expression and cellular proliferation.[18] Sensitive detection of miRNAs still remains a great challenge ascribed to the little size, ultralow expression, and high sequence homology. For meeting the corresponding sensitivity requirements, the polymerization/nicking reaction (PNR) has drawn our attention as an emerging and promising nucleic acid signal amplification strategy.[19] With the trigger of the model target, substantial replicating copies of output can be generated with assistance of the synthesis component deoxy-ribonucleoside 5′-triphosphate mixture (dNTPs), the polymerization of DNA polymerase, and the nicking reaction of endonuclease.[20] Different from the PNR, DNA nanomachines are artificially designed self-assemblies, in which the walking strands move progressively and autonomously along with the predetermined tracking strands.[21] Compared with one-dimensional and 2D DNA nanomachines, three-dimensional (3D) DNA nanomachines have better amplification behaviors, higher DNA loading capacity, and enrichment capability of secondary targets.[22] However, traditional 3D DNA nanomachines are usually liable to be confronted with limited movement space, probable derailment, and difficult separation of output.[23] Therefore, improving the operation mode and amplification efficiency of 3D DNA nanomachines remains a significant need. As a new type of 3D DNA nanomachines, the dual-particle 3D DNA roller is featured with relative movement of walking particles (WPs) and tracking particles (TPs), which can meet the demands of vast wing area, high operation rate, and inhibition of derailment. Composed of the PNR and dual-particle 3D DNA roller, the cascaded quadratic amplification strategy can attain exponential accumulation of output, as well as higher amplification efficiency.

In this regard, we propose an "ON−OFF−ON" PEC biosensor for detecting miRNA 1246 (as a model analyte) by integrating the cascaded quadratic amplification strategy and Au NPs/PTCDA as the excellent photoelectric material. Au NPs were investigated systematically at different electrodeposition times on PTCDA to explore their photosensitive effects. The as-prepared biosensor exhibited outstanding analytical performances toward miRNA 1246. This work shows the potential applications of 3D DNA nanomachines in bioanalysis involving protein testing and nucleic acid determination. Also, it provides a new channel to research photosensitization of Au NPs to organic photoelectric materials.

EXPERIMENTAL SECTION

Materials and Reagents. PTCDA, ascorbic acid (AA, 99%), and 6-mercapto-1-hexanol (MCH) were obtained from Sigma-Aldrich (St. Louis, MO, USA). $[Fe(CN)_6]^{3-/4-}$ solution, 0.1 M phosphate buffer (PB, pH 7.4), 10 mM TE buffer (Tris−HCl, 1 mM EDTA, pH 8.0), and 10 mM STE buffer (Tris−HCl, 150 mM NaCl, 1 mM EDTA, pH 8.0) were used (details in Supporting Information). dNTPs, Nb.BbvCI nicking endonuclease, and Klenow fragment (KF) polymerase were purchased from New England Biolabs, Inc. (Beijing, China). All oligonucleotides were obtained from Shanghai Sangon Biological Engineering Technology and Services Co., Ltd. (Shanghai, China). They are listed as follows: assist strand 1 (AS1): 5′-ATC CTT CCT CAG CTT CAA CAG ACC TCA GCC ATA TCT AAA ATC CAT T -3′, assist strand 2 (AS2): 5′−NH_2−$(CH_2)_6$- AAA AAT CAT CCC TCA GCT TCA ACA GAC CTC AGC CTG CTC CAG AT-3′, amine-hairpin DNA1 (H1): 5′-AAG CCC TGT TTT TT*T AAAGC*↓ ***T GAGG***GC TTC AAC AGA CCT CA −$(CH_2)_6$−NH_2-3′, track: 5′-*CCT CAG CTT TAT* TTT TTT TCT CCC GAA GTT G −$(CH_2)_6$−NH_2-3′, assist strand 3 (AS3): 5′-GCT TTA AAA AAA CAG GAA TA**G AGG CGC TGC CCC CAC CAT GAG C**-3′, and capture probe (CP): 5′−NH_2−$(CH_2)_6$- TTA TAA CCT GTT TTT TT-3′. For H1, the underlined sections belonged to the stem parts and the bold segment corresponded to the Nb.BbvCI cleavage sequence (5′-GC↓T GAG G-3′). The italic part was designed to hybridize with track. For AS3, the bold section was the template of Au NCs. H1 was annealed before use by heating to 95 °C for 5 min and then cooled down to 25 °C at a rate of 1 °C/min. The other reagents were of analytical grade. Double distilled water was used throughout the whole work.

Instrumentation. The PEC plots were recorded by a CHI 440A electrochemical workstation, which was integrated with PEAC 200A (Tianjin AiDa Hengsheng Technology Co., Ltd., China) for visible-light irradiation. In a three-electrode system, a bare or modified glassy carbon electrode (GCE, Φ = 4 mm), Ag/AgCl (sat. KCl), and a platinum wire were applied as the working electrode, the reference electrode, and the counter electrode, respectively. It was periodically set off−on−off with 10−20−10 s, and each modified electrode was immersed into 4.0 mL of PB (0.1 M, pH 7.4) containing 50 mM AA (electron donor) for PEC measurements. Other instrumentation details are listed in Supporting Information.

Fabrication of the Dual-Particle 3D DNA Roller. AS3-Au NCs,[24] MBs-AS2, MBs-H1, and MBs-track[25] were prepared according to the literature (see Supporting Information). PNR cycle: the same volumes of AS1 (300 nM), MBs-AS2 (5 μM), miRNA 1246 with various concentrations, KF polymerase (0.75 U/μL), Nb. BbVCI (1.5 U/μL), and dNTPs (3600 μM) were incubated at 37 °C for 2 h and heated to 80 °C for 20 min to inactivate enzymes. After magnetic separation, the supernatant was collected as output 1. Dual-particle 3D DNA rolling process: the same volumes of output 1, MBs-H1 (5 μM), MBs-track (5 μM) and Nb. BbVCI (1.5 U/μL) were

https://doi.org/10.1021/acs.analchem.1c01816
Anal. Chem. 2021, 93, 10947−10954

Scheme 1. (A) Preparation of the Dual-Particle 3D DNA Roller and (B) Stepwise Modification of the Electrode

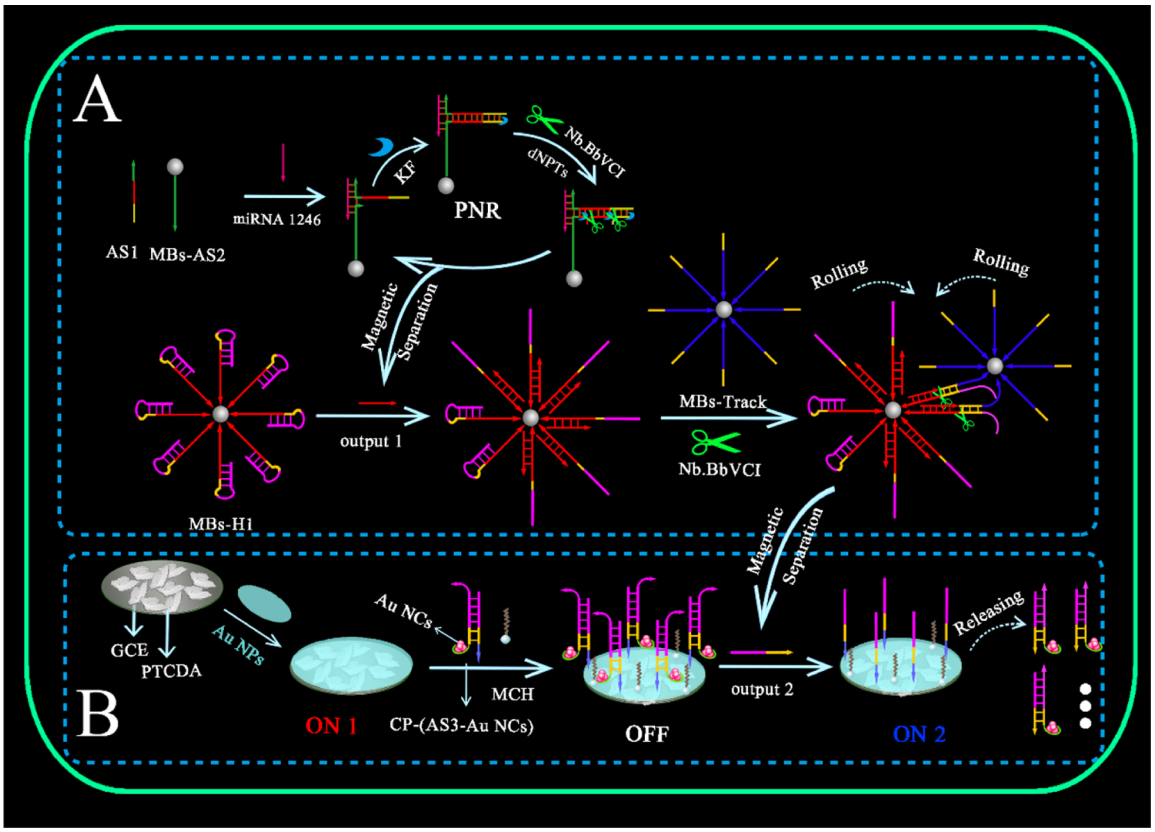

incubated at 37 °C for 2 h and then heated to 80 °C for 20 min to inactivate enzymes. The last product supernatant (output 2) was collected through the magnetic separation process (Scheme 1A).

Construction of the Modified Electrodes. Each clean GCE was coated by 10 μL of 20 μM PTCDA aqueous solution (denoted as PTCDA/GCE). After drying in the air, the PTCDA/GCE was immersed into 1% $HAuCl_4$ solution for potentiostatic electrodeposition at −0.2 V for 15 s to form a Schottky junction (Au NPs/PTCDA/GCE, ON 1). Meanwhile, AS3-Au NCs and CP were hybridized at 37 °C for 2 h to form CP-(AS3-Au NCs). Then, 20 μL of CP-(AS3-Au NCs) and 10 μL of MCH were added onto the modified electrode successively (MCH/CP-(AS3-Au NCs)/Au NPs/PTCDA/GCE, OFF). Finally, 20 μL of output 2 was added to take AS3-Au NCs away from the electrode by hybridization (output2/MCH/CP-(AS3-Au NCs)/Au NPs/PTCDA/GCE, ON 2). The electrode was washed with double distilled water after each modification to remove the nonspecific absorbed molecules and dried in the air (Scheme 1B).

RESULTS AND DISCUSSION

Characterization of Nanomaterials. The scanning electron microscopy (SEM, Figure 1A) and transmission electron microscopy (TEM, Figure S1A) images of PTCDA show irregular quadrate-shaped molecular islands. The UV-illuminated image (insert of Figure 1A) shows that PTCDA possesses the characteristic of emitting fuchsia fluorescence under the irradiation of a UV lamp (365 nm). The X-ray photoelectron spectrum (Figure 1B−D) and Fourier transform infrared spectrum (Figure 1E) show characteristic peaks of C−O and C═O, indicating the presence of anhydride in PTCDA. The specific analysis of XPS and FTIR is listed in Tables S1 and S2, displaying the other bond characteristics. X-ray diffraction (XRD) displays the semiconductor crystalline properties of PTCDA (Figure 1F); the characteristic peaks at 12.3, 17.2, 20.2, 24.8, 26.0, and 27.5° correspond to the crystal faces of (110), (021), (112), (022), (200), and (310), respectively. The highest occupied molecular orbital (HOMO) energy levels and the lowest unoccupied molecular orbital (LUMO) energy levels were evaluated to be −5.49 and −2.99 eV, respectively (Figure S3 and Table S3). The experimental results are in accordance with the ones of the density functional theory (Figure S3F). The Mott−Schottky measurement was performed at the frequency of 10 Hz. The plot exhibits a positive slope, implying that PTCDA is consistent with the behavior of a typical n-type semiconductor (Figure 1G).[26] The n-type PTCDA with an appropriate optical band gap of 2.5 eV owns inherent outstanding PEC performances.

The TEM image (Figure S1B) shows that the equally distributed Au NCs are close to spheres with a mean diameter of 2.1 nm. In addition, the particle sizes of MBs-AS2, MBs-H1, and MBs-track are very close to those of the MBs (Figure 1H).

Initial PEC Signal Obtained by Regulating the Electrodeposition Time. Figures 2A−H and S2 exhibit the SEM images of Au NPs at varying electrodeposition times on PTCDA and bare GCE. The changes in crystal seeds are similar: with the extension of the electrodeposition time, the crystal seeds gradually accumulated. Meanwhile, the increasing electrodeposition time leads to a higher PEC current owing to the synergetic effect of LSPR and the Schottky junction. However, when the electrodeposition time is 35 s, a decreased photocurrent is observed (Figure 2I), hinting at the strong

https://doi.org/10.1021/acs.analchem.1c01816
Anal. Chem. 2021, 93, 10947−10954

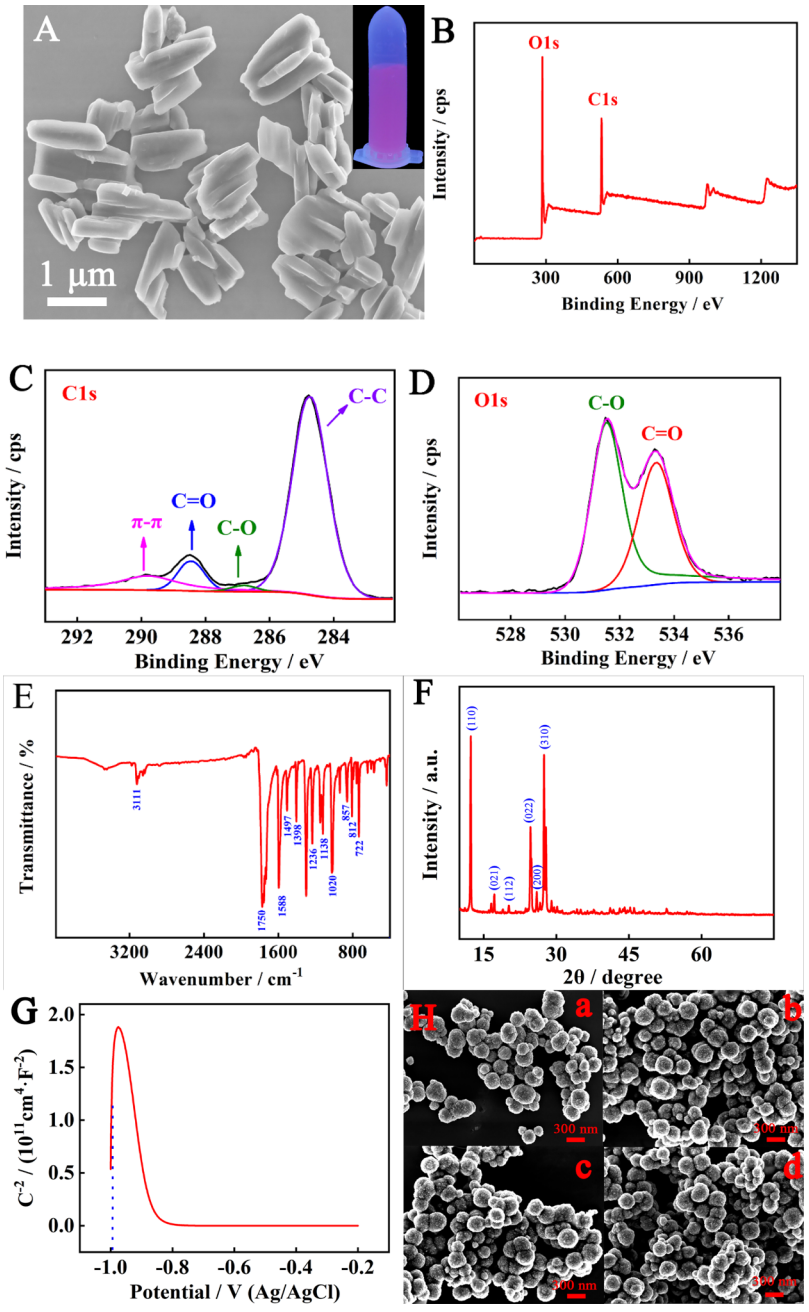

Figure 1. (A) SEM image (insert: photograph under the illumination of UV light at 365 nm), XPS patterns of (B) full scale, (C) C 1s and (D) O 1s, (E) FTIR, (F) XRD spectra, and (G) Mott−Schottky plots of PTCDA. (H) SEM images of (a) MBs, (b) MBs-AS2, (c) MBs-H1, and (d) MBs-track.

steric hindrance coming from the saturated Au NPs attached to PTCDA, which results in the reduced light harvest efficiency of PTCDA. In consideration of a fundamental tradeoff between the synergetic effect and steric effect, the optimized electrodeposition time is selected as 35 s. Interestingly, the recorded photocurrent is around fourfold higher than that of the single PTCDA substrate. In addition, the calculated effective electroactive surface area of PTCDA and Au NPs/PTCDA are 4.54 and 15.56 mm^2, respectively (Figure S4). Thus, Au NPs/PTCDA with a larger surface area can facilitate electron transfer and help fabricate the PEC biosensing substrate with high electroactivity.

Reason for PEC Signal Enhancement of Au NPs/PTCDA. The reason for the enhanced PEC signal of Au NPs/PTCDA is discussed as follows. First, the plasmonic nanostructures of Au NPs help form resonant SPs corresponding to a photon flux, resulting in remarkable enhancement of the electromagnetic field on the surface of the plasmonic nanostructures.[27,28] That is to say, when photons interact with Au NPs, the surface conduction electrons collectively oscillate to generate LSPR. Second, in the visible light region, the extinction coefficient of Au NPs is 4−5 orders of magnitude higher than that of organic dye stuff, which provides favorable prerequisite for plasmon sensitization.[29] Third, the formation of Schottky junction pumps electrons and holes induced in or near this area to move in opposite directions. It is favorable for the accumulation of space charges, generating a relatively large built-in field, in which the charge separation of photoinduced

https://doi.org/10.1021/acs.analchem.1c01816
Anal. Chem. 2021, 93, 10947−10954

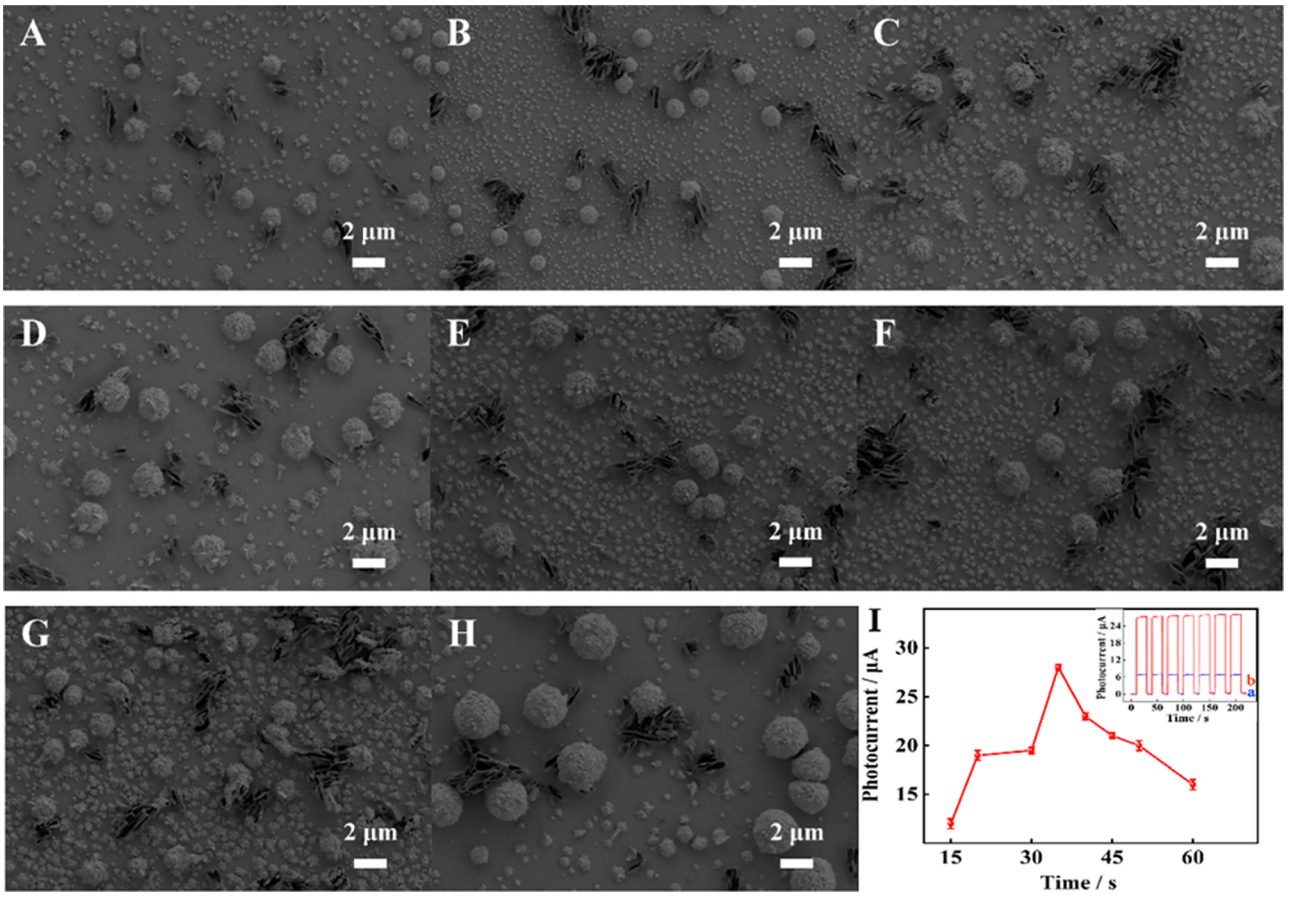

Figure 2. SEM images of Au NPs on the PTCDA substrate for varying electrodeposition times of (A) 15, (B) 20, (C) 30, (D) 35, (E) 40, (F) 45, (G) 50, and (H) 60 s. (I) Effect of the electrodeposition time of Au NPs on the PEC signal of PTCDA. Insert: PEC responses of (a) PTCDA and (b) PTCDA after the electrodeposition of Au NPs for 35 s.

charge carriers is facilitated and the recombination process is suppressed. In brief, the synergetic effect of LSPR and the Schottky junction can make it capable for harvesting visible light, extending the lifetime of electron−hole pairs, activating the photogenerated carriers, minimizing the charge carrier recombination, and enhancing photoreaction rate, which realize a significantly increased PEC response in comparison with PTCDA.[30]

Principle of the PEC Biosensor. Composed of the PNR and dual-particle 3D DNA roller, the cascaded quadratic amplification strategy has realized exponential signal amplification. Based on the toehold-mediated strand displacement reaction, a general "ON-OFF-ON" PEC biosensor has been designed for ultrasensitive detection of miRNA 1246 (Scheme 1). Such a universal PEC biosensing system includes five single-stranded DNAs: AS1 and AS2 in the PNR cycle, CP and AS3 in the toehold-mediated strand displacement reaction, and track in the dual-particle 3D DNA roller. Since AS1 and AS2 separately contain part of target miRNA 1246 recognition sequences, they can hybridize perfectly with miRNA 1246 to form a three-way junction structure. The two hybridization domains complementary to the Nb.BbvCI cleavage sequences are also incorporated in AS1 and AS2. Owing to only four complementary bases, AS1 and AS2 are kinetically inhibited in the absence of miRNA 1246. However, AS1, AS2, and miRNA 1246 can hybridize to generate a three-way junction structure with the trigger of miRNA 1246, forming a recessing 3′—end of AS2 in the duplex region. Taking AS1 and AS2 as templates, the 3′—end of AS2 is isothermally extended with the polymerization of KF polymerase. As the newly generated sequences of AS2 contained the Nb.BbcCI-specific sequence (5′-GC↓T GAG G-3′), it is cleaved to release plentiful output1. Meanwhile, the cleaved AS2 can be elongated by KF polymerase and cleaved by Nb.BbcCI again to achieve the PNR cycle.

In H1, the active regions are locked into the hairpin structure through intramolecular hybridization. H1 is elaborately designed with three functional segments. The first is the 3′—overhanging end (red), which is bound with output1, unfolding the hairpin structure of H1. The second section (yellow) is used to combine with track to operate the DNA nanomachine. The second segment is designed partially to be locked into the stem of H1 to kinetically inhibit the simultaneous assembly of H1 and track without the participation of output 1. The Nb.BbvCI cleavage sequence (5′-GC↓T GAG G-3′) is included in both the first and the second domains. The third domain (violet) is used as a trigger sequence to initiate toehold-mediated strand displacement on the modified electrodes. The second and the third parts are hybridized with the presynthesized AS3-Au NCs. With the trigger of output1, based on the polymerization of KF polymerase and cleavage of Nb.BbcCI, WPs and TPs are rolled oppositely and simultaneously to complete the operation of this DNA roller, liberating abundant output2.

AS3 is divided into two functional sections: one (green) is the synthesis template of Au NCs. The other contains the

https://doi.org/10.1021/acs.analchem.1c01816
Anal. Chem. 2021, 93, 10947−10954

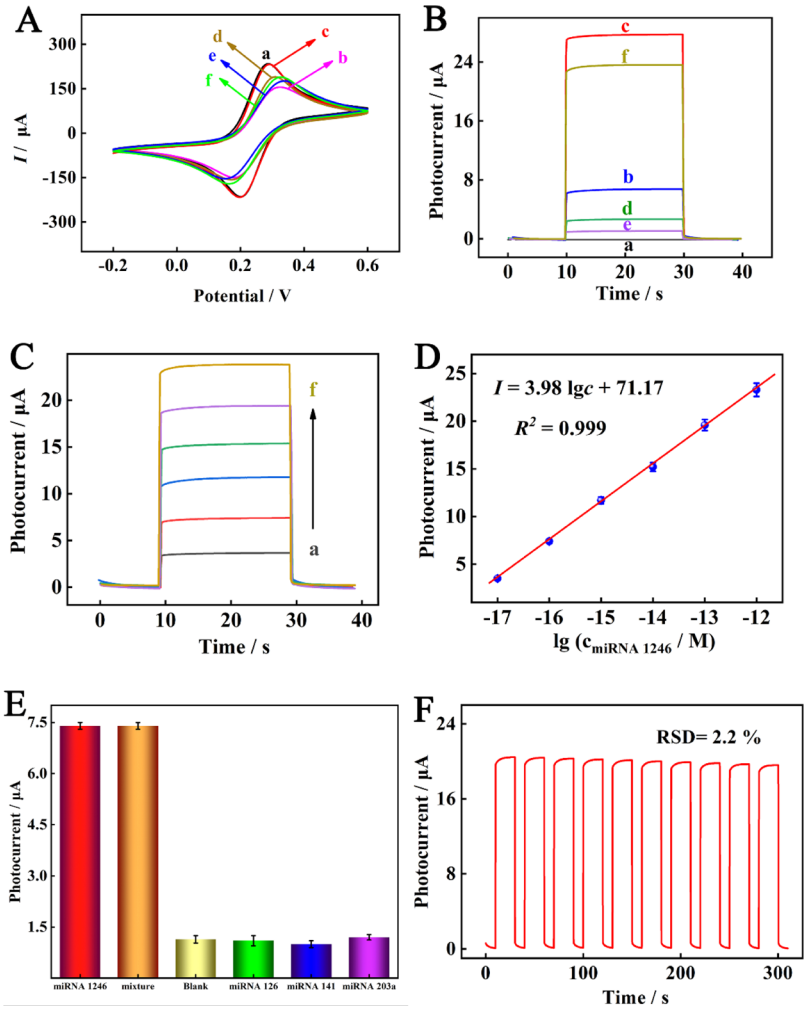

Figure 3. (A) Cyclic voltammograms (CVs) and (B) PEC responses of stepwise modified electrodes: (a) bare GCE, (b) PTCDA/GCE, (c) Au NPs/PTCDA/GCE, (d) CP-(AS3-Au NCs)/Au NPs/PTCDA/GCE, (e) MCH/CP-(AS3-Au NCs)/Au NPs/PTCDA/GCE, (f) output2/MCH/CP-(AS3-Au NCs)/Au NPs/PTCDA/GCE. (C) Photocurrents of miRNA 1246 with diverse concentrations, (a) 10 aM, (a) 100 aM, (c) 1 fM, (d) 10 fM, (e) 100 fM, and (f) 1 pM. (D) Calibration plot of the photocurrents vs the logarithmic concentration of miRNA 1246. (E) Selectivity and (F) stability of the proposed biosensor.

violet and yellow parts, which are partial and complete complementary sequences with CP and output2, respectively. The presynthesized CP-(AS3-Au NCs) remains a toehold, which can bind with output2 to complete the toehold-mediated strand displacement reaction. Once the quencher AS3-Au NCs are liberated, the PEC signals are recovered and the quantitative detection of miRNA 1246 can be achieved.

Electrochemical and PEC Characterization of the Stepwise Modified Electrodes. Figure 3A shows the cyclic voltammetry (CV) measurements. The peak current recorded on the PTCDA/GCE is remarkably lower than that of the GCE (curve a,b) because of the poor conductivity of the semiconductor. After electrodeposition of Au NPs, the peak current obviously increases owing to the excellent electron transfer ability of Au NPs (curve c). After the incubation of CP-(AS3-Au NCs), a decreased peak current is observed (curve d) ascribed to the repulsion effect between $[Fe(CN)_6]^{3-/4-}$ and the negatively charged double stranded DNA. After the electrode is blocked by MCH, a sequentially decreased peak current is exhibited (curve e). When output2 is incubated, the peak current restores as the quencher Au NCs are taken away from the modified electrodes (curve f). The results of electrochemical impedance spectroscopy (EIS, Figure S6) are consistent with the CV results.

The PEC performances of the stepwise-modified electrodes were also investigated (Figure 3B). The photocurrent close to zero appears on the GCE (curve a), while an obvious photocurrent of 7 μA is gained on the PTCDA/GCE (curve b). Because of the effective photosensitization of Au NPs, around fourfold higher photocurrent of 28 μA (curve c, ON 1) than PTCDA/GCE is recorded on Au NPs/PTCDA/GCE. After the incubation of CP-(AS3-Au NCs), the PEC signal dramatically decreases (curve d). The PEC response further decreases with the addition of MCH (curve e, OFF). While output2 takes the quencher CP-(AS3-Au NCs) away from the electrode, the photocurrent recovers (curve f, 23 μA, ON 2).

Analytical Behaviors of the Prepared PEC Biosensor. Under the optimized experimental conditions (Figure S5), the analytical performances of the developed biosensor were assessed by quantitative detection of miRNA 1246 with different concentrations from 10 aM to 1 pM (Figure 3C,D). The PEC responses show a positive correlation with the logarithmic concentrations of miRNA 1246. The regression equation is I = 3.98 lg$c$ + 71.17 (R^2 = 0.999), and the limit of

https://doi.org/10.1021/acs.analchem.1c01816
Anal. Chem. 2021, 93, 10947−10954

detection (LOD) is 3.1 aM. In comparison with other biosensors for miRNA detection, the as-proposed biosensing platform shows a relatively lower LOD and a wider dynamic range (Table S4). Meanwhile, compared with some biosensors developed by the derivatives of PTCDA, this photoelectric plasmon-enhanced biosensor exhibits higher calibration sensitivity (Table S5). These encouraging results imply recommendable analytical behaviors of this biosensing system, which is due to the enhanced initial PEC intensity resulting from the synergistic effect of LSPR and the Schottky junction of Au NPs.

Selectivity and Stability. Some miRNAs containing miRNA 126, miRNA 141, and miRNA203a with the same concentration of 10 fM were employed as interferences to explore the selectivity of this biosensor. As depicted in Figure 3E, the photocurrent for target miRNA 1246 (100 aM) was much higher than that of the blank solution (absence of miRNA 1246). When the biosensor was used to analyze these interfering substances separately, the recorded PEC intensity was very close to the blank solution. For the mixture solution including all the interferences (each of 10 fM) and miRNA 1246 (100 aM), the PEC response was close to the photocurrent of miRNA 1246. These consequences illustrated the excellent selectivity of this biosensor. The stability was investigated by the analysis of miRNA 1246 (100 fM) in 4 mL of 0.1 M PB (pH 7.4). The recorded photocurrent was barely constant under consecutive PEC measurements for 10 cycles, and the relative standard deviation (RSD) was 2.2%, suggesting the outstanding stability of the proposed biosensing platform (Figure 3F).

Mechanism of Photocurrent Generation. Scheme 2A shows the PEC responses of PTCDA with and without AA; a strong PEC signal is observed with AA, indicating that AA serves as an electron donor in the photoelectric process. Scheme 2B illustrates a strong photoluminescence (PL) response of PTCDA at around 665 nm. After the introduction of AA, the intensity of the PL peak decreases obviously, implying that the recombination of photogenerated electron−hole pairs is greatly suppressed in comparison to PTCDA. Namely, the charge separation and transfer efficiency are greatly promoted with the assistance of AA.[31,32]

The possible mechanism of this biosensor is illustrated in Scheme 2C. The electrons at the HOMO of PTCDA could inject into the LUMO under illumination (process a). The inherent LSPR-induced localized electric field amplification of Au NPs could boom the photon absorption of PTCDA in the visible region, and the generated hot electrons by LSPR excitation could transfer to the LUMO of PTCDA (process b). They further drifted to the GCE (process c) and could be recorded by an electrochemical workstation. AA as a sacrificial electron donor could provide numerous electrons (process d) to the HOMO of PTCDA (process e) to guarantee continuity of the photocurrent. When Au NCs were introduced, the electrons could be excited from the HOMO of Au NCs to the LUMO (process f) and the photogenerated holes in the HOMO could be neutralized by the electron donor AA (process g). Meanwhile, the electrons in the LUMO could be consumed by dissolved oxygen (O_2) to generate the superoxide radical ($O_2^{-\bullet}$). Therefore, Au NCs could compete to expend AA and irradiation against PTCDA, bringing about an obviously decreased PEC signal.

Practical Applicability in Serum Samples. The standard addition method was utilized to study the practical application of the as-prepared biosensor. MiRNA 1246 with varying concentrations from 10 aM to 100 fM was spiked in the pretreated serum samples. As shown in Table S6, the recovery was in the range of 96.0−103.6% and the RSD ranged from 1.2 to −3.8%, implying its feasibility in clinical research.

Scheme 2. (A) PEC Responses of PTCDA (a) with and (b) without AA; (B) PL Emissions (λex = 532 nm) of (a) PTCDA and (b) Mixture of PTCDA and AA; (C) Possible Mechanism of the "ON−OFF−ON" PEC Plasmon-Enhanced Biosensor

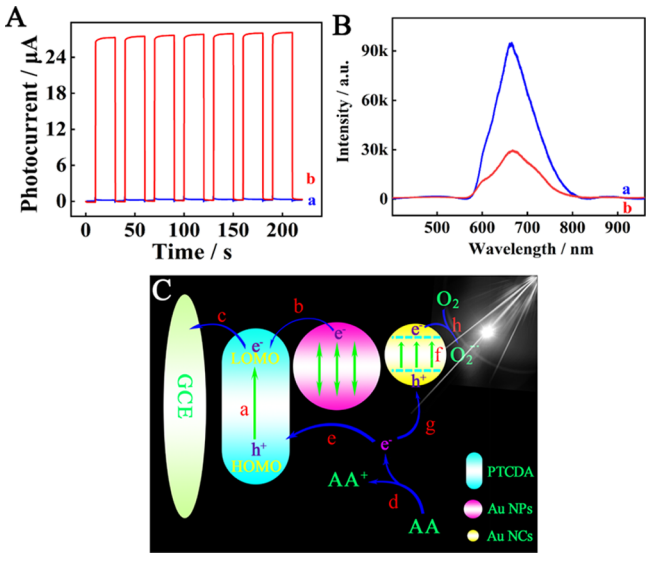

CONCLUSIONS

In this work, based on the remarkable photosensitization of Au NPs to PTCDA and the good quenching effect of Au NCs to PTCDA, taking miRNA 1246 as a model analyte, the universal "ON−OFF−ON" PEC sensing platform has been developed combined with the cascaded quadratic amplification strategy of the PNR and dual-particle 3D DNA roller. Due to the synergistic effect of LSPR and the Schottky junction, the Au NPs/PTCDA/GCE achieves fourfold higher signal than that of the pristine PTCDA. The high initial PEC signal ensures the excellent analytical sensitivity. The proposed dual-particle 3D DNA roller makes some impressive improvements on the basis of traditional DNA nanomachines. The developed sensing platform exhibits excellent analytical performances in healthy human serum samples. This strategy extends the application of organic optoelectronic materials and provides potential possibility to detect other biomarkers by choosing appropriate target units.

ASSOCIATED CONTENT

Supporting Information

The Supporting Information is available free of charge at https://pubs.acs.org/doi/10.1021/acs.analchem.1c01816.

Materials and reagents, instrumentation, synthesis of Au NCs templated with AS3 (AS3-Au NCs), synthesis of MBs-AS2, MBs-H1, and MBs-track, TEM images of PTCDA and Au NCs, SEM images of Au NPs for varying electrodeposition time, HOMO and LUMO, electroactive surface area of PTCDA and Au NPs/PTCDA, condition optimization, EIS characterization of

https://doi.org/10.1021/acs.analchem.1c01816
Anal. Chem. 2021, 93, 10947−10954

the stepwise modified electrodes, XPS analysis of PTCDA, FTIR analysis of PTCDA, electrochemical data and calculated energy levels, comparison of miRNA detection with other detection methodologies, comparison of the calibration sensitivity with previous reports, and detection of miRNA 1246 in serum samples (PDF)

AUTHOR INFORMATION

Corresponding Author

Yingzi Fu − *Key Laboratory of Luminescence Analysis and Molecular Sensing (Southwest University), Ministry of Education, School of Chemistry and Chemical Engineering, Southwest University, Chongqing 400715, China;* orcid.org/0000-0003-4894-8549; Phone: +86-023-68252277; Email: fyzc@swu.edu.cn

Authors

Fangjing Mo − *Key Laboratory of Luminescence Analysis and Molecular Sensing (Southwest University), Ministry of Education, School of Chemistry and Chemical Engineering, Southwest University, Chongqing 400715, China*

Jiang Guo − *Key Laboratory of Luminescence Analysis and Molecular Sensing (Southwest University), Ministry of Education, School of Chemistry and Chemical Engineering, Southwest University, Chongqing 400715, China*

Min Chen − *Key Laboratory of Luminescence Analysis and Molecular Sensing (Southwest University), Ministry of Education, School of Chemistry and Chemical Engineering, Southwest University, Chongqing 400715, China*

Hui Meng − *Key Laboratory of Luminescence Analysis and Molecular Sensing (Southwest University), Ministry of Education, School of Chemistry and Chemical Engineering, Southwest University, Chongqing 400715, China*

Complete contact information is available at: https://pubs.acs.org/10.1021/acs.analchem.1c01816

Notes

The authors declare no competing financial interest.

ACKNOWLEDGMENTS

This work was supported by the National Natural Science Foundation of China (22077105), Natural Science Foundation Project of CQ CSTC (cstc2020jcyj-msxmX0854), and Graduate Scientific Research and Innovation Foundation of Chongqing (CYB20089), China.

REFERENCES

(1) Hodes, G.; Cahen, D.; Manassen, J. *Nature* **1976**, *260*, 312−313.
(2) Kenney, M. J.; Gong, M.; Li, Y.; Wu, J. Z.; Feng, J.; Lanza, M.; Dai, H. *Science* **2013**, *342*, 836−840.
(3) Liu, Z.; Sun, K.; Li, X.; Li, L.; Zhang, H.; Chi, L. *J. Phys. Chem. Lett.* **2019**, *10*, 4297−4302.
(4) Deng, H.-M.; Zhu, M.-H.; Huang, L.-J.; Chai, Y.-Q.; Liu, X.-R.; Yuan, R.; Yuan, Y.-L. *Anal. Chem.* **2019**, *91*, 12468−12475.
(5) Huang, L.; Zhang, L.; Yang, L.; Yuan, R.; Yuan, Y. *Biosens. Bioelectron.* **2018**, *104*, 21−26.
(6) Huang, L.; Deng, H.; Zhong, X.; Zhu, M.; Chai, Y.; Yuan, R.; Yuan, Y. *Biosens. Bioelectron.* **2019**, *145*, 111702−111707.
(7) Li, X.-H.; Antonietti, M. *Chem. Soc. Rev.* **2013**, *42*, 6593−6604.
(8) Li, X.; Zhu, H.; Wang, K.; Cao, A.; Wei, J.; Li, C.; Jia, Y.; Li, Z.; Li, X.; Wu, D. *Adv. Mater.* **2010**, *22*, 2743−2748.
(9) Dobbs, W.; Suisse, J.-M.; Douce, L.; Welter, R. *Angew. Chem., Int. Ed.* **2006**, *45*, 4179−4182.
(10) Zhu, W.; Michalsky, R.; Metin, Ö.; Lv, H.; Guo, S.; Wright, C. J.; Sun, X.; Peterson, A. A.; Sun, S. *J. Am. Chem. Soc.* **2013**, *135*, 16833−16836.
(11) Wang, C.; Nie, X.-G.; Shi, Y.; Zhou, Y.; Xu, J.-J.; Xia, X.-H.; Chen, H.-Y. *ACS Nano* **2017**, *11*, 5897−5905.
(12) He, F.; Meng, A.; Cheng, B.; Ho, W.; Yu, J. *Chin. J. Catal.* **2020**, *41*, 9−20.
(13) Chen, M.; Mo, F.; Meng, H.; Wang, C.; Guo, J.; Fu, Y. *Anal. Chem.* **2021**, *93*, 2464−2470.
(14) Chen, M.; Meng, H.; Mo, F.; Guo, J.; Fu, Y. *Biosens. Bioelectron.* **2021**, *191*, 113475−113481.
(15) Fu, B.; Zhang, Z. *Small* **2018**, *14*, 1703610−1703616.
(16) Lapp, A. S.; Duan, Z.; Marcella, N.; Luo, L.; Genc, A.; Ringnalda, J.; Frenkel, A. I.; Henkelman, G.; Crooks, R. M. *J. Am. Chem. Soc.* **2018**, *140*, 6249−6259.
(17) Liu, C.; Wang, K.; Luo, S.; Tang, Y.; Chen, L. *Small* **2011**, *7*, 1203−1206.
(18) Chen, Y.; Wang, X. *Nucleic Acids Res.* **2020**, *48*, D127−D131.
(19) Li, D.; Zhang, T.; Yang, F.; Yuan, R.; Xiang, Y. *Anal. Chem.* **2020**, *92*, 2074−2079.
(20) Li, X.; Xu, X.; Song, J.; Xue, Q.; Li, C.; Jiang, W. *Biosens. Bioelectron.* **2017**, *91*, 631−636.
(21) Hu, Q.; Li, H.; Wang, L.; Gu, H.; Fan, C. *Chem. Rev.* **2019**, *119*, 6459−6506.
(22) Zhang, H.; Xu, X.; Jiang, W. *Chem. Sci.* **2020**, *11*, 7415−7423.
(23) Jung, C.; Allen, P. B.; Ellington, A. D. *Nat. Nanotechnol.* **2016**, *11*, 157−163.
(24) Liu, G.; Shao, Y.; Ma, K.; Cui, Q.; Wu, F.; Xu, S. *Gold Bulletin* **2012**, *45*, 69−74.
(25) Zhang, Y.; Chai, Y.; Wang, H.; Yuan, R. *Anal. Chem.* **2019**, *91*, 14368−14374.
(26) Jiang, Z. W.; Zou, Y. C.; Zhao, T. T.; Zhen, S. J.; Li, Y. F.; Huang, C. Z. *Angew. Chem., Int. Ed.* **2020**, *59*, 3300−3306.
(27) Shi, R.; Cao, Y.; Bao, Y.; Zhao, Y.; Waterhouse, G. I. N.; Fang, Z.; Wu, L.-Z.; Tung, C.-H.; Yin, Y.; Zhang, T. *Adv. Mater.* **2017**, *29*, 1700803−1700809.
(28) Zhan, C.; Wang, Z. Y.; Zhang, X. G.; Chen, X. J.; Huang, Y. F.; Hu, S.; Li, J. F.; Wu, D. Y.; Moskovits, M.; Tian, Z. Q. *J. Am. Chem. Soc.* **2019**, *141*, 8053−8057.
(29) Li, C.; Lu, W.; Zhu, M.; Tang, B. *Anal. Chem.* **2017**, *89*, 11098−11106.
(30) Wang, M.; Ye, M.; Iocozzia, J.; Lin, C.; Lin, Z. *Adv. Sci.* **2016**, *3*, 1600024−1600037.
(31) Song, G.; Gong, W.; Cong, S.; Zhao, Z. *Angew. Chem., Int. Ed.* **2021**, *60*, 5505−5511.
(32) Yang, S.; Yao, J.; Quan, Y.; Hu, M.; Su, R.; Gao, M.; Han, D.; Yang, J. *Light Sci. Appl.* **2020**, *9*, 117−123.